Journal of Tropical Resources and Sustainable Science
Website : http://journal.umk.edu.my/index.php/jtrss/
eISSN : 2462-2389
Vol: 14, Issue 1, 2026, 182-190
DOI: https://doi.org/10.47253/jtrss.v14i1.2152

RESEARCH ARTICLE

Roles of Silver Particle Immobilised in Polysulfone Mixed Matrix Membrane on Flux Enhancement and Antibacterial Properties

Khairul Anwar Mohamad Said[1*], Shaiza Asif[2], Norsuzailina Mohamed Sutan[1], Ibrahim Yakub[1], Mohamed Afizal Mohamed Amin[1,2], Md Rezaur Rahman[1,2] and Sinin Hamdan[1]

[1] Faculty of Engineering, Universiti Malaysia Sarawak, 94300 Kota Samarahan, Sarawak, Malaysia
[2] Unimas Water Center (UWC), Universiti Malaysia Sarawak, 94300 Kota Samarahan, Sarawak, Malaysia

ARTICLE HISTORY
Received: 16 October 2025
Accepted: 15 December 2025
Online: 31 March 2026

KEYWORDS
Silver,
Antibacterial,
Immobilised,
Polysulfone,
Mixed matrix membrane

☒ * **CORRESPONDING AUTHOR**
Khairul Anwar Mohamad Bin Said
Faculty of Engineering,
Universiti Malaysia Sarawak,
94300, Kota Samarahan,
Sarawak, Malaysia.
Email: mskanwar@unimas.my

ABSTRACT

A mixed matrix membrane immobilised with silver particles has been reported to possess antibacterial properties. Nevertheless, the presence of a foreign particle such as silver inside the membrane matrix could introduce a flux resistance that reduces the water permeation. Therefore, this study investigated the influence of silver particles on the membrane by varying the silver particle dosage. The silver immobilised mixed matrix membrane was analysed using scanning electron microscopy (SEM), Fourier Transform Infrared (FTIR), X-ray diffraction (XRD), Brunauer, Emmett, and Teller (BET), and porosity tests to identify the effect of silver particles on membrane physicochemical properties. The membrane performance was evaluated by water flux and antibacterial tests. The water flux test revealed that adding silver particles in the membrane improved the water flux up to ~22 L/m^2.h at 1.0 wt% silver content (PPAG1.0) compared to the pristine (PPAG0) membrane, which reported ~5 L/m^2.h of flux. Further increase in silver dosage led to flux reduction, in which the membrane with 2.0 wt% (PPAG2.0) recorded ~8 L/m^2.h flux. The antibacterial test indicated that the silver content in the membrane was directly proportional to the ability of a membrane to impede *E. coli* growth. The PPAG2.0 membrane exhibited the largest diameter of inhibition ring at 27.0 mm, while the pristine membrane did not inhibit *E. coli* growth. Hence, the optimum silver content in the membrane was identified at 1.0 wt% based on the PPAG1.0 membrane performance, exhibiting an inhibition diameter of 19.0 mm and ~22 L/m^2.h flux.

1. INTRODUCTION

Polysulfone (PSF) is composed of a polyether chain with multiple sulfone groups. This thermoplastic polymer is produced from bisphenol A and sodium bisulphite by a polycondensation reaction. The chemical structure is similar to polycarbonate, but with higher molecular weights and temperature ranges, and improved chemical and hydrolytic resistance. Thus, a PSF-based membrane has a hydrophobic surface that is susceptible to foulants due to the van der Waals bond, hydrogen bonding, and electrostatic attraction (Prihandana et al., 2022).

A PSF hydrophobic surface implies that the accumulation of foulant on the surface will lead to pore blocking and cake forming, reducing the overall flux (Zambare et al., 2017). Therefore, PSF membranes must demonstrate a hydrophilic surface characteristic to mitigate the drawbacks. One of the approaches to develop this feature is by introducing particles such as titanium dioxide, zinc oxide, and silver, which assist the membrane in minimising fouling and increasing the membrane rejection performance (Alias et al., 2020; Mollahosseini et al., 2012).

Silver nanoparticles have been used in many applications, from home appliances (refrigerators, washing machines) to water treatment systems (Li et al., 2008). Silver is known to be a hypoallergenic material that possesses optical and thermal characteristics, and is considered non-toxic. Silver nanoparticles have been studied for the antibacterial properties against pathogens such as *Escherichia coli*, *Pseudomonas aeruginosa*, and *Staphylococcus aureus* (Huq et al., 2022). Nonetheless, the exact mechanism of action of silver ions and nanoparticles is poorly understood.

Researchers have theorised that silver binds to the cell membrane of the bacteria and disrupts their metabolism, leading to cell death. Silver nanoparticles have also been found to be effective against certain antibiotic-resistant bacteria. Azhar et al. (2020) investigated the influence of bio-silver immobilised PSF membranes on humic acid rejection and water flux. Their findings revealed that the relationship of

bio-silver content in the membrane is directly proportional to its flux. The membrane with 1.0 wt% of bio-silver displays an impressive flux exceeding 300 L/m2.h, while the pristine membrane registered flux at the sub-200 region (Azhar et al., 2020). Meanwhile, the antibacterial assessment revealed that the pristine membrane did not display any inhibition ring, suggesting the absence of antibacterial activity. In contrast, all membranes consisting of bio-silver exhibited the inhibition ring, in which the membrane with 1.0 wt% bio-silver possesses the largest inhibition area at ~18 mm^2 (Azhar et al., 2020).

Besides silver application in ultrafiltration membrane, Bian et al. (2022) fabricated an RO membrane with a polyamide thin film that consisted of silver modified with unique nanospheres. The water flux performance indicated that the silver-modified nanosphere improved the overall flux with an average of ~50 L/m2.h, while the pristine RO membrane only averaged at ~30 L/m2.h (Bian et al., 2022). Despite the high flux, the pristine RO membrane outperformed RO with modified silver in the salt rejection test, although at a slim margin. All membranes reported an excellent salt rejection of more than 98% (Bian et al., 2022). Therefore, the inclusion of silver in the membrane, either for ultrafiltration or RO, has improved the membrane flux and the rejection performance.

In the present study, the effect of silver particle dosage on the polyethersulfone membrane physicochemical properties and antibacterial resistance against *E. coli* were investigated. The silver particle content varied from 0.5 to 2.0 wt%, and the influence of the silver particles on the membrane was analysed based on the cross-section and surface morphology, pore characteristics, and antibacterial properties via the disk diffusion method. At the end of this study, the optimum amount of silver particles in polyethersulfone was identified based on the water flux and antibacterial performance.

2. MATERIALS AND METHODS

2.1. Materials

The PSF pellets, with an average Mw* of 35,000 (Sigma-Aldrich, USA), were used as polymers for membrane synthesis. The solvent used for membrane fabrication was N-Methyl-2-pyrrolidone (NMP) supplied by Sigma-Aldrich (USA). The nanohybrid materials were formed using silver nitrate ($AgNO_3$, 98%), sodium hydroxide (NaOH, 0.1M), and ethanol solutions obtained from Merck. The Luria-Bertani broth and agar acquired from Sigma-Aldrich were used to grow and culture bacteria for the characterisation of the membrane antibacterial properties.

The primary goal of this study was to investigate the role of silver particles in the antibacterial hybrid membrane, with the incorporation of silver nitrate ($AgNO_3$) ranging from 0.5 to 2.0 wt.% in the hybrid membrane structures. The NMP solvent was used to dissolve the polymers at a ratio of 15:85, and the nanomaterials ($AgNO_3$) percentage varied between 0.5 and 2.0 wt.% during the membrane fabrication (Table 1).

Table 1: PSF membrane compositions.

Membrane Type	$AgNO_3$ Wt%	PSF Wt%	NMP Wt%
PPAG0	-	15.0	85.0
PPAG0.5	0.5	15.0	83.7
PPAG1.0	1.0	15.0	83.2
PPAG1.5	1.5	15.0	82.7
PPAG2.0	2.0	15.0	82.2

Notes: PPAG0: PSF membrane solution without any additives, PPAG0.5: PSF membrane solution with 0.5 wt% $AgNO_3$, PPAG1.0: PSF membrane solution with 1.0 wt% $AgNO_3$, PPAG1.5: PSF membrane solution with 1.5 wt% $AgNO_3$, and PPAG2.0: PSF membrane solution with 2.0 wt% $AgNO_3$.

2.2. Membrane Fabrication

The PSF membranes in the form of a flat sheet were prepared using the phase inversion technique, by incorporating $AgNO_3$ as the functional nanomaterial. The combination of these functional additives was targeted to enhance the membrane performance regarding water flux, membrane porosity, and the antibacterial capability towards *E. coli*.

Before the dope solution was prepared, the PSF polymer was oven-dried at 103°C (Panasonic MOV Laboratory Oven) to remove the moisture content for 24 h. At this stage, a flat sheet form of the PSF membrane was fabricated through a wet phase inversion method. Approximately 15.0 g of PSF was mixed with NMP (85.0 ml) in a 250 ml beaker to obtain a pure PSF membrane solution without any additives (PPAG0). The mixture was then mechanically blended for 8 h to form a homogenous solution at 60°C. The lid of the container was kept closed with aluminium foil to prevent solvent evaporation during stirring.

Composite membranes (PPAG0.5, PPAG1.0, PPAG1.5 and PPAG2.0) were prepared by adding $AgNO_3$ into the solution (Table 1). Subsequently, the homogeneous membrane dope solution was cast on a 210 mm x 297 mm glass plate with a casting blade. The membrane was left to evaporate for 1 min, and the membrane with a glass plate was immersed in a water bath at room temperature to ensure a complete phase separation. The flat sheet membrane was rinsed thrice in the coagulation bath (2.5 L of distilled water) to remove the solvent and dried at room temperature for 24 h.

2.3. Membrane Characterisation

2.3.1 Fourier transform infrared (FTIR)

The FTIR spectroscopy (Bunker Equinox 50) was used to determine the presence of functional groups in the nanohybrid membranes containing a diverse measure of silver loadings. The FTIR spectrum was analysed in the range of 4000 to 400 cm^{-1} with 40 scans for each sample and 4 cm^{-1} resolution. The wavelength transmittance value represents the functional groups in the membranes.

2.3.2 Scanning electron microscopy (SEM)

The surface and cross-section morphology of the prepared membranes were examined by using SEM (JSM-6390LA, JEOL, Japan), operating at 15 kV. The composite membrane samples were cut into approximately 1 cm^2 and immersed in liquid nitrogen for 1 min, followed by cryogenic fracture to provide even surface breakage on the membrane samples. The cracked membrane samples were then attached to a sample holder and coated with a thin layer of gold under vacuum for 20 s using an Auto Fine Coater (JOEL JFC 1600, Japan). The top surface and the cross-sectional morphology of each membrane were evaluated, and the average pore size was manually measured.

2.3.3 X-ray diffraction (XRD)

The XRD of the membrane was performed using an X–ray diffractometer (Philips PW 1710, UKM) with a Cobalt target at 40 kV in 10°– 80° θ. The adsorbent sample was prepared by compressing the membrane in the cassette sample holder without any adhesive.

2.3.4 Brunauer, Emmett, and Teller (BET) surface area

The BET (Autosorb iQ-MP, UNIMAS) gas adsorption theory is generally used to determine the surface area in high specification surface materials. The specific surface area of the adsorbent is measured by the adsorption of nitrogen at 77 K using the molecular area of nitrogen at 0.162 nm^2, and the BET surface area (SBET) of the adsorbent was determined using a surface area analyser.

2.3.5 Porosity

Each membrane was cut into approximately 2 cm^2 and soaked in deionised water for 24 h to determine the porosity. The weight of the wet membrane was recorded after wiping away the water on the membrane surface. Subsequently, the membranes were oven-dried at 75°C for 24 h to obtain the dry weight. The membrane thickness was measured by using a digital calliper and was used to calculate the porosity with a gravimetric method (see Eq. 1).

$$\varepsilon(\%) = \frac{w_W - w_d}{A \cdot \delta \cdot \rho} \times 100\% \quad (1)$$

Where,

ε = porosity of the membrane,

A = membrane area (cm^2),

δ = membrane thickness (cm),

ρ = pure water density (0.998 g/ cm^3)

2.4. Membrane performance

2.4.1 Pure water flux

The performance of the synthesised membrane was characterised by measuring the pure water flux. The pure water flux was tested with an ultrafiltration setup using a laboratory-scale dead-end system, Stirred Ultrafiltration Cell (Model 8050, Millipore Corp., Bedford, MA) at room temperature with a 50 ml-internal volume under an active membrane surface area of 13.4 cm^2. In this test, the membranes with different concentrations of silver nitrate were examined to obtain the best-performing membrane under different compositions.

Each membrane with a radius of 44.5 mm was immersed in the deionised water prior to the filtration process for 5 mins. Subsequently, the membrane was positioned between two steel plates and sealed with an O-ring. The feed solution for the pure water flux test was deionised water, and stirred using a magnetic stirrer placed within the membrane-stirred cell system. The pure water flux of each membrane was measured at a 10-min filtration interval and compacted at 2 bars. The experiment was conducted at room temperature under a 2-bar pressure supplied by the compressed gas. The pure water flux of each membrane was determined using Eq. 2.

$$\text{Flux, } J_0 = \frac{\text{Volume of water permeation (V)}}{\text{Membrane area (A)X Permeation time(t)}} = \frac{V}{A\Delta t} \quad (2)$$

Where,

J_0 is the pure water flux ($L/m^2.h$)

V is the volume of water permeated (L)

A is the membrane area (m^2)

Δt is the permeation time (h)

2.4.2 Antibacterial test on membrane

The fabricated membranes were evaluated for

antibacterial properties by using the disk diffusion method. Firstly, the bacterial culture media were prepared with Lura Bertani (LB) stock powder and bacteriological agar. Approximately 5 g of bacteriological agar and 25 g of LB stock were blended in 1000 ml of deionised water. The agar solution was then autoclaved at a temperature of 121°C for 20 mins, and cooled to room temperature for approximately 30 mins before being poured into petri dishes. The petri dishes refrigerated until use.

The cotton swab was immersed in the *E. coli* solution before the cells were spread homogeneously onto the agar plates. The sterilised composite membranes were then placed on the LB agar and incubated for 24 h at 37°C. Subsequently, the inhibition zone on the membrane surface was determined by measuring the difference between the membrane area and the area of the ring formed around the sample.

3. RESULT AND DISCUSSION

3.1 Membrane morphology

3.1.1 SEM analysis

Figure 1 illustrates the surface characteristics of the membrane, which indicated that all membranes had distinctive pores. The PPAG0 and PPAG1.0 membranes exhibited the least pore formation across the surface. Nonetheless, the pores on PPAG0 were larger and non-uniform, while PPAG1.0 showed a similar pattern but with smaller pores that were evenly distributed. Meanwhile, PPAG2.0 demonstrated a uniform pore distribution that occupied most of the membrane surface, with a mixture of large and small pores. Although the observation was based on qualitative estimation, the observation remains comparable, indicating that PPAG0 possesses larger pore dimensions, while PPAG1.0 demonstrates a membrane structure with smaller pores.

The SEM analysis of the membrane surfaces revealed the pore distribution, with PPAG1.5 comprising more large pores than other membranes. The PPAG2.0 membrane consisted of well-distributed pores that varied in size compared to other membranes. According to Mino et al. (2021), compatibilities between the polymer-rich phase and the solid surface are the main driver that contributes to the pore formation in the membrane. The study investigated the formation of porous structures on membrane surfaces via thermal-induced phase separation (TIPS) and concluded that high or low compatibility between those factors will lead to low surface porosity on the membrane surface. Meanwhile, a balance or similar compatibilities between the polymer-rich phase and the solid surface will form a porous membrane surface (Mino et al., 2021).

Vatanpour et al. (2022) investigated the inclusion of boron nitride/silver/graphene oxide in polyethersulfone membranes on the physicochemical properties. The pristine polyethersulfone membrane demonstrated a dense surface with no apparent pore formation, while the inclusion of nanoparticles has assisted the formation of pores across the membrane surface (Vatanpour et al., 2022). Although the addition of nanoparticles should lead to a more porous structure, the study found that the increment of nanoparticles content up to 0.5 wt% increased solution viscosity, which severely affected the pore formation (Vatanpour et al., 2022).

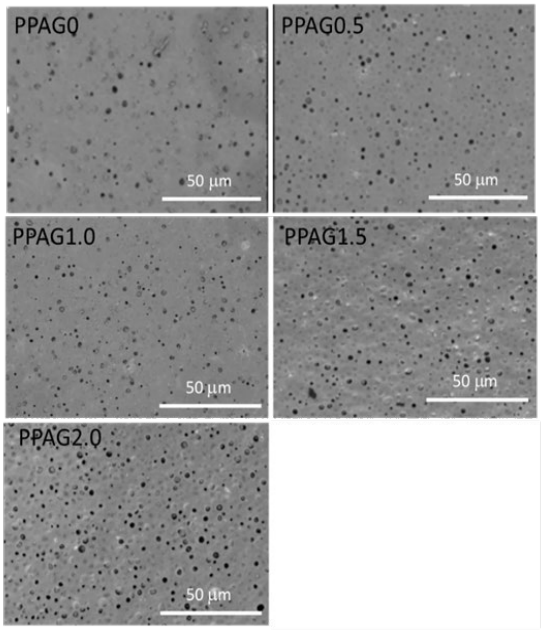

Figure 1: Membrane surface morphology (×1500): (a) PPAG0, (b) PPAG0.5, (c) PPAG1.0, (d) PPAG1.5, and (e) PPAG2.0.

Figure 2 presents the cross-section of the membrane at 1500 magnification. All membranes were fractured with the assistance of liquid nitrogen. Based on the cross-section, all membranes exhibited a sponge-like structure, and the difference among the images was the compactness of the structure. The PPAG2.0 cross-section illustrates a more uniform pore on the sponge structure, whereas PPAG1.0 and PPAG1.5 had a dense sponge structure. Meanwhile, PPAG0 and PPAG0.5 indicated a porous structure similar to PPAG2.0 (see Figure 2). A similar finding was reported by Little Flower et al. (2019), where the membrane with the highest percentage of polymer (18% Ag-PSF) displayed a sponge-like structure, while the membrane with the lowest polymer content (9% Ag-PSF) had a dense structure (Little Flower et al., 2019). The study on the effect of silver nanoparticle blend with PSF membrane suggested that the outcomes can be attributed to dope solution viscosity, although the general rule would be that an increase in polymer content will lead to a viscous solution (Little Flower et al., 2019).

Despite silver being a hydrophobic material,

excessive hydrophilic particles in the membrane could also be detrimental to the membrane structure. Zeng et al. (2022) investigated the effect of fullerol (a hydrophilic material) on the PSF ultrafiltration membrane, in which the membrane was fabricated using phase inversion, resulting in a mixed matrix membrane. The membrane cross-section showed that the structure was finger-like for the pristine membrane (pure PSF) and the membrane with 2.0% fullerol (Zeng et al., 2022). Higher fullerol inclusion (2.5%) caused the membrane structure to become sponge-like (Zhang et al., 2022). These findings indicated that a hydrophilic material may also influence the membrane structure formation, particularly at high dosages. The fabricated membrane demonstrated a similar structure to that of the study by Zhang et al. (2022) at a high dosage of silver.

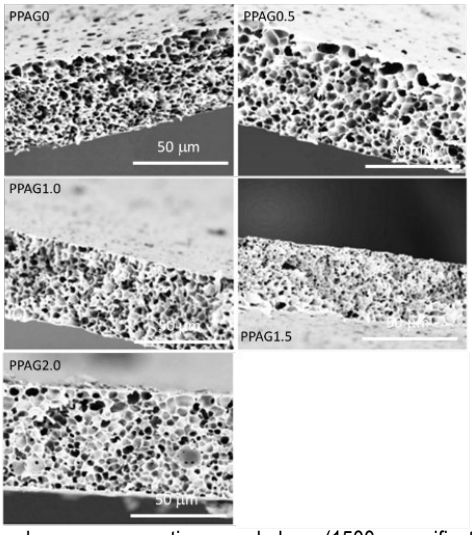

Figure 2: Membrane cross-section morphology (1500 magnification, 50 µm) (a) PPAG0, (b) PPAG0.5, (c) PPAG1.0, (d) PPAG1.5, (e) PPAG2.0.

Table 2 shows the average pore size of the membrane, revealing that the PPAG1.5 membrane has the largest pore, while the PPAG0 membrane has the smallest pore. PPAG2.0, which has a well-distributed pore on its surface, has an average pore size of 3.26 nm. In terms of pore size, the smallest pore size is more favourable, allowing it to filter more incoming material based on the size exclusion principle. Fahrina et al. (2022) functionalized a polyethersulfone (PES) membrane with polyether glycol-silver nanoparticles (PEG-Agnp) for a biofouling study. Guerout–Elford–Ferry equation was used to estimate the membrane porosity, and their finding indicates that the addition of silver nanoparticles will positively affect the pore size by increasing its comparison to the pristine membrane and the membrane coupled with PEG (Fahrina et al., 2022; Mohamad Said et al., 2022). However, adding more than 3 wt% silver nanoparticles has been shown to limit pore size growth.

Fahrina et al. (2022) report that a membrane with 3 wt% silver nanoparticles has a pore diameter of ~225 nm, while adding 5 and 7 wt% silver shows that the pore size decreases to ~180nm and ~165nm, respectively. The decreasing trends indicate that silver inside the membrane affects the pore size. A similar trend was observed in our study, in which the pristine membrane (PPAG0) has the smallest pore size, while the addition of silver particles led to an increment in pore size.

Table 2: PPAG membrane average pore size.

Composite Membrane	Average value for pore size (nm)
PPAG0	2..24±0.01
PPAG0.5	3.13±0.01
PPAG1.0	3.18±0.01
PPAG1.5	4.15±0.1
PPAG2.0	3.26±0.01

Notes: PPAG0: PSF membrane solution without any additives, PPAG0.5: PSF membrane solution with 0.5 wt% $AgNO_3$, PPAG1.0: PSF membrane solution with 1.0 wt% $AgNO_3$, PPAG1.5: PSF membrane solution with 1.5 wt% $AgNO_3$, and PPAG2.0: PSF membrane solution with 2.0 wt% $AgNO_3$

Table 3: PPAG membrane porosity.

Composite Membrane	Porosity (%)
PPAG0	6.5
PPAG0.5	15.5
PPAG1.0	70.9
PPAG1.5	46.9
PPAG2.0	27.1

Notes: PPAG0: PSF membrane solution without any additives, PPAG0.5: PSF membrane solution with 0.5 wt% $AgNO_3$, PPAG1.0: PSF membrane solution with 1.0 wt% $AgNO_3$, PPAG1.5: PSF membrane solution with 1.5 wt% $AgNO_3$, and PPAG2.0: PSF membrane solution with 2.0 wt% $AgNO_3$.

Table 3 shows the membrane porosity quantified via the gravimetric method. The PPAG0 membrane registered the lowest porosity at 6.5%, and the trend was shown to increase with the addition of silver from 0.5 to 1.0 wt%, while further addition led to a reduction in membrane porosity. PPAG1.0 membrane shows the most porous structure at 70.9%, while PPAG1.5 and PPAG2.0 membranes show declined membrane porosity at 46.9 and 27.1%, respectively. Vatanpour et al. (2022) modified the PES with boron nitride/silver/graphene oxide (FBN-GO-Ag) for wastewater treatment applications. Based on their findings, the pristine membrane (bare PES) has the lowest overall porosity at 66.8%. The addition of nanoparticles increases the membrane porosity, suggesting that the nanoparticle content is directly

proportional to membrane porosity (Vatanpour et al., 2022). Vatanpour et al. (2022) report that the membrane with the highest content of nanoparticles (1 wt% FBN-GO-Ag) has the most porous structure at 81.3% with a pore size of 11.8 nm. In comparison, our study shows that PPAG2.0, with the highest content of silver, has an average porosity (27.1%) and pore size of 3.26 nm.

3.2 Physical and Chemical properties

3.2.1 Functional group

The FTIR analysis was conducted on a mixed matrix membrane containing silver particles to identify the effect of silver particle dosage on the membrane functional group. Table 4 lists the functional group in a membrane with silver particles, indicating two bonds were associated with nitrogen, mainly at 692 cm-1 and 1585.49 cm-1, corresponding to -NH wagging vibration and N-H bond (Pereira et al., 2015). Both the nitrogen-linked bonds were sourced from nitrate, which is part of the silver nitrate compound. Jyoti et al. (2016) synthesised silver nanoparticles from a stinging nettle plant and characterised the synthesised silver with several analytical equipment, including FTIR. The findings indicated that the silver nanoparticle demonstrated an absorption band at 2921, 1631, 1240, 1043, and 596 cm^{-1} (Jyoti et al., 2016), coinciding with the current study (2912, 1585, 1149, and 692 cm^{-1}). The slight shift in the peak value was attributed to the interaction of silver particles with the PSF membrane.

Gan et al. (2020) immobilised carbon quantum dots and silver in a PSF membrane for dye removal. The FTIR spectra of the modified membrane revealed a small peak at 550.12 cm^{-1}, representing the silver oxide that interacted with the carbon quantum dots (Gan et al., 2020). Therefore, besides the -NH wagging vibration from the silver nitrate at 692 cm^{-1}, the peak is potentially caused by the presence of silver oxide. In conclusion, the occurrence of a peak at 692 and 1585 cm^{-1} suggested the presence of silver inside the membrane matrix in this study, improving the flux and contributing to the antibacterial properties. Figure 3 illustrates the FTIR spectra of the membrane immobilised with different dosages of silver particles.

Table 4: Functional groups present in the PPAG membranes.

Wavelength (cm^{-1})	Bond
629.44	-NH wagging vibration
873.75	C-H aromatic
1149.57	Symmetric stretching vibration O=S=O
1585.49	N-H bond
2912.543	C-H symmetric vibration

Figure 3: FTIR results for PPAG0.5, PPAG1.0, PPAG1.5 and PPAG2.0.

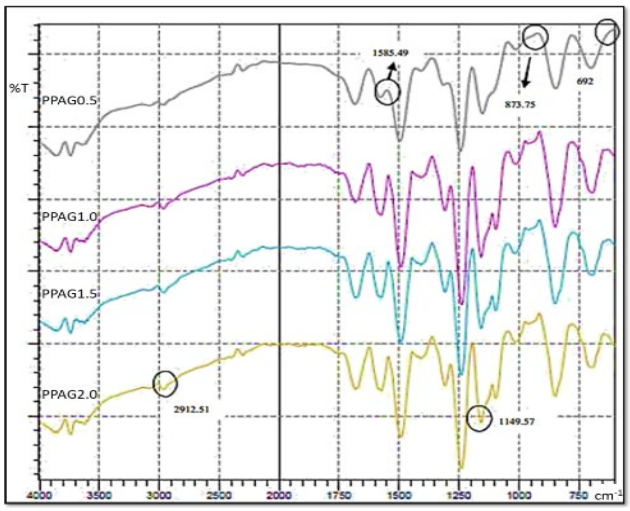

3.2.2 Crystallisation

Figure 4 depicts the crystallisation of pristine and modified membranes. As expected, all membranes displayed an amorphous structure with no apparent sharp peak. The most notable peak was at 2θ = 13°, supporting the claim that all membranes possess an amorphous structure. Although the XRD chart did not show an apparent peak at 2θ = 44.3°, which is based on the standard JCPDS (04-0783) for silver, the peak indexed by Theivansathi and Alagar (2011) indicated that other peaks associated with silver particles were observed at 2θ = 38.3°, 64.7°, 77.5°, and 81.7°. The 2θ = 77.5° from silver peak indexing can be represented by hkl of 311 (Theivasanthi & Alagar, 2011). Among the alternative peaks in the current study, the peak at 2θ = 77.5° was observed in the PPAG2.0 membrane. The higher silver content in the membrane, the more prominent the peak is at 2θ = 77.5°.

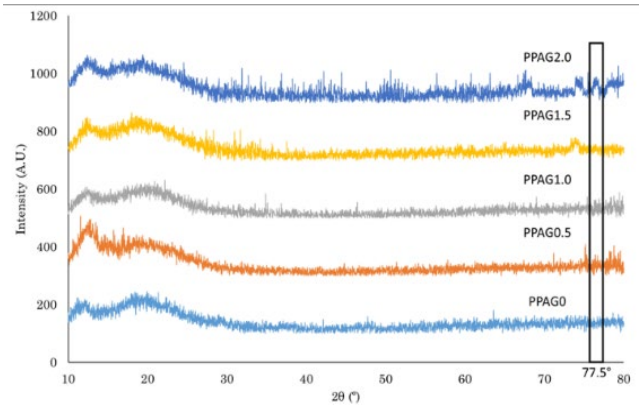

Figure 4: XRD Analysis for PPAG0.5, PPAG1.0, PPAG1.5 and PPAG2.0.

3.2.3 BET surface area

Table 5 lists the membrane surface area analysed via BET. The PPAG0 membrane exhibited the highest surface area, where the silver addition reduced the membrane surface

area proportionally to the dosage. Hence, the PPAG2.0 membrane with 2.0 wt% silver demonstrated a low surface area compared to PPAG0.5 with 0.5 wt% silver, where the difference exceeded 250 m^2/g. Despite the apparent differences between the membrane surface area, particularly when comparing the highest and the lowest, the surface area was still high compared to earlier studies. For example, Parsamehr et al. (2019) fabricated a cross-linked graphene oxide supported on a cellulose acetate membrane. The membrane recorded a dense structure with low porosity at 0.0017%, which was estimated numerically based on d-spacing and graphene oxide sheet width (Parsamehr et al., 2019). The BET analysis in this study revealed that the membrane surface was only 5.62 m^2/g, which was expected in a low porosity membrane. The membrane cross-section confirmed the BET and porosity analysis, demonstrating that the membrane had a dense structure without finger-like or sponge-like structure.

Table 5: Surface area of all membranes.

Membrane	Nap
PPAG0	19.37±0.5
PPAG0.5	1216.38 ± 1.37
PPAG1.0	856.267 ± 0.02
PPAG1.5	731.19 ± 0.83
PPAG2.0	678.94 ± 0.21

Notes: PPAG0: PSF membrane solution without any additives, PPAG0.5: PSF membrane solution with 0.5 wt% $AgNO_3$, PPAG1.0: PSF membrane solution with 1.0 wt% $AgNO_3$, PPAG1.5: PSF membrane solution with 1.5 wt% $AgNO_3$, and PPAG2.0: PSF membrane solution with 2.0 wt% $AgNO_3$

3.4 Performance

3.4.1 Water flux

Figure 5 depicts the membrane water flux, which revealed the PPAG1.0 membrane with the highest flux (22.25 L/m2.h) while the PPAG0 or pristine membrane had the slowest flux (5.53 L/m2.h). The slow flux exhibited by PPAG0 was caused by the compact and dense structure, as depicted by the cross-section (see Figure 2). A more porous structure was one of the factors that contributed to the high flux. Moreover, the membrane surface morphology indicated that PPAG0 lack pore distribution across the surface, while PPAG1.0, PPAG1.5, and PPAG2.0 membranes have a clear distribution of pores. Despite the porous structure and clear pores, the PPAG2.0 membrane registered low membrane flux (~3 L/m2.h), different from the PPAG0 membrane. Based on Table 3, the porosity of the PPAG2.0 membrane was low compared to the porosity of the PPAG1.0 membrane. At 27.1% porosity, the PPAG2.0 membrane structure lacks an interlink pore inside the matrix that facilitates water permeation. Likewise, the PPAG0 membrane exhibited 6.5% porosity, resulting in the lowest flux among membranes.

Based on the BET surface area (see Table 5), PPAG0 high surface area was not reflected in the water flux performance, indicating that surface area did not influence water permeation across the membrane. Similarly, there was a ~400 m^2/g difference in water flux between PPAG1.0 (856 m2/g) and PPAG0 (1216 m2/g). Despite the large differences in surface area, the PPAG1.0 membrane reported the highest water flux, indicating that the property that contributes to membrane water flux is porosity.

A similar trend was observed in a study by Prihandana et al. (2022), which utilised silver particles in nanoflake form to add value to an ultrafiltration PSF membrane. The addition of 0.1 wt% silver nanoflakes significantly improved water permeability over the pristine PSF membrane, with a difference of ~30 L/m2.h.bar (Prihandana et al., 2022). Nevertheless, further addition of silver nanoflakes drastically reduced water permeability to match the pristine membrane. Prihandana et al. (2022) also reported that the sudden increase in water permeability with silver nanoflakes in the membrane was contributed to by the increase in hydrophilicity. Beyond the optimum silver nanoflake content, the extra particles cause pore blockage, creating resistance for water to permeate and reducing the overall flux performance.

Besides ultrafiltration membranes, silver particles have been applied in forward osmosis membranes. For instance, Wu et al. (2022) explored the effect of biogenic silver particles immobilised in a forward osmosis membrane on curbing internal concentration polarisation. The biogenic silver particle was synthesised with the assistance of bacteria (Rai et al., 2021). In the water flux test, the addition of biogenic silver particles contributed to an increase in water flux, with the highest record at ~14 L/m2.h (0.1 wt% biogenic silver). The water flux performance was reduced at a higher content of biogenic silver (0.25wt%) (Wu et al., 2022). Nonetheless, all membranes with biogenic silver surpass the water flux performance of the pristine forward osmosis membrane.

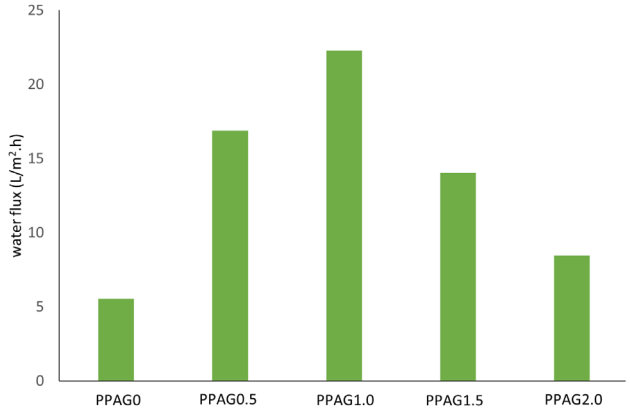

Figure 5: Flux changes of the composite membranes (PPAG0 to CM F).

3.4.2 Antibacterial test

Table 6 details the inhibition zone diameter of each membrane against *E. coli,* while Figure 6 illustrates the image inhibition zones on agar plates. As expected, membranes with higher silver dosage demonstrated superior inhibition, with a larger inhibition zone. The PPAG0 did not inhibit *E. coli,* demonstrating the lack of an inhibition zone. The ring effect around the PPAG0 membrane identifies the inhibition zone, which generally indicates no *E. coli* colony. Therefore, no disinfection activity occurs without the ring effect on PPAG0, including under the membrane area.

There was a ~10 mm difference between the membrane with the highest and the lowest silver content. The largest inhibition zone was recorded by PPAG2.0 (2.0 wt% silver) at 27.0 mm, while PPAG0.5 (0.5 wt% silver) only recorded 17.5 mm. In this test, the silver particles inside the membrane leached out of the membrane and prevented the growth of *E. coli* in the surroundings. The mechanism of silver preventing the growth of bacteria such as *E. coli* is based on the release of Ag^+ ions (Zhao et al., 2022). The silver was doped with hesperidin and pectin to assist in the production of Ag^+ ions. The study discovered six pathways that contribute to the *E. coli* disinfection mechanism. The production of Ag^+ ions will lead to the presence of reactive oxygen species (ROS), responsible for bacterial death (Zhao et al., 2022).

Table 6: Diameter of inhibition zone for all membranes.

Composite Membrane	Diameter (mm)
PPAG0	17.0 (actual diameter of the membrane)
PPAG0.5	17.5
PPAG1.0	19.0
PPAG1.5	21.0
PPAG2.0	27.0

Notes: PPAG0: PSF membrane solution without any additives, PPAG0.5: PSF membrane solution with 0.5 wt% $AgNO_3$, PPAG1.0: PSF membrane solution with 1.0 wt% $AgNO_3$, PPAG1.5: PSF membrane solution with 1.5 wt% $AgNO_3$, and PPAG2.0: PSF membrane solution with 2.0 wt% $AgNO_3$

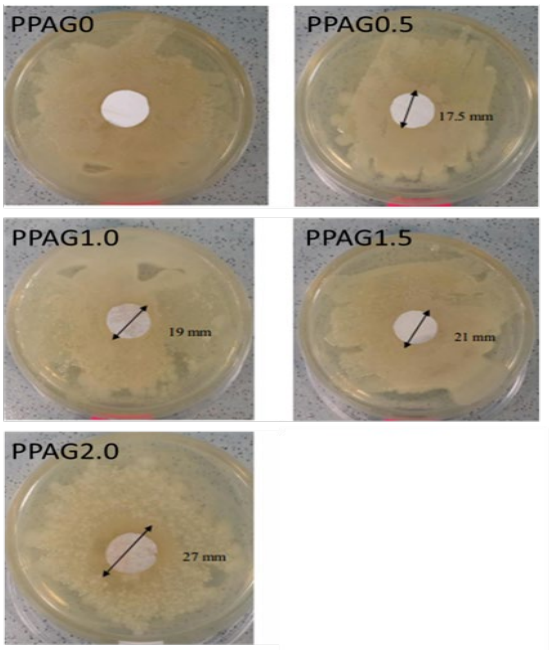

Figure 6: Inhibition zone on agar plates. PPAG0: PSF membrane solution without any additives, PPAG0.5: PSF membrane solution with 0.5 wt% $AgNO_3$, PPAG1.0: PSF membrane solution with 1.0 wt% $AgNO_3$, PPAG1.5: PSF membrane solution with 1.5 wt% $AgNO_3$, and PPAG2.0: PSF membrane solution with 2.0 wt% $AgNO_3$.

Zhao et al. (2022) extended their investigation by conducting SEM imaging to observe the effect of silver particles on the *c*cell. Upon attachment of silver particles on the bacterial cell surface, the rod-shaped *E. coli* changed to a different shape entirely, with the surface appearing to be damaged, with a distinguished silver particle presence on its surface (Zhao et al., 2022). He et al. (2022) incorporated silver nanoparticles attached to nanofibrils into nanofiltration membranes for desalination applications. In the antibacterial test, the Kirby-Bauer test resulted in the ring effect by the membrane against *E. coli,* which indicated that the membrane containing silver nanoparticles has a significant inhibition zone. In contrast, a pristine membrane does not indicate any *E. coli* inhibition (He et al., 2022). The conclusion derived from this study was that the PPAG0 membrane would be prone to biological contamination, while the silver membrane would withstand and purify the feed from bacterial growth.

4. CONCLUSION

The silver particle immobilised membrane was fabricated at different silver particle contents from 0.5 to 2.0 wt%. The presence of silver inside the membrane matrix significantly altered the membrane structure and properties, including the surface morphology, cross-section, porosity, and surface area. These changes in membrane morphology influenced the membrane performance in the water flux and antibacterial tests. In the water flux experiment, PPAG1.0 membrane (1.0 wt% silver) recorded the highest flux (~22

L/m2.h), while PPAG0 (pristine) membrane registered the lowest flux (~5.5 L/m2.h). Meanwhile, more than 1.0 wt% silver particles in membranes caused the water flux to decline, but the values remained higher than those of the PPAG0 membrane. The antibacterial test indicated that the amount of silver particles in the membrane was directly proportional to the diameter of the inhibition zone. The PPAG2.0 membrane (2.0 wt% silver) exhibited the largest inhibition zone (27 mm), while PPAG0.5 (0.5 wt% silver) demonstrated the smallest inhibition zone (17.5 mm). In conclusion,1.0 wt% silver particles contributed to an increase in membrane overall performance in water flux and antibacterial properties, which is crucial for sustainable membrane fabrication.

ACKNOWLEDGMENT

The authors acknowledge the VC-High Impact Research Grant for funding this study (UNI/F02/VC-HIRG/85517/P12-02/2022). The authors also extend their appreciation to the Research, Innovation and Enterprise Centre (RIEC), Universiti Malaysia Sarawak (UNIMAS), for managing the research activity.

STATEMENTS AND DECLARATIONS

The authors declare no conflict of interest in the publication of this work.

DATA AVAILABILITY

The data that support the study findings are available from the corresponding author upon reasonable request.

REFERENCES

Alias, S. S., Harun, Z., Azhar, F. H., Ibrahim, S. A., & Johar, B. (2020). Comparison between commercial and synthesized nano flower-like rutile TiO_2 immobilized on green super adsorbent towards dye wastewater treatment. Journal of Cleaner Production, 251, 119448. https://doi.org/10.1016/j.jclepro.2019.119448

Azhar, F. H., Harun, Z., Yusof, K. N., Alias, S. S., Hashim, N., & Sazali, E. S. (2020). A study of different concentrations of bio-silver nanoparticles in polysulfone mixed matrix membranes in water separation performance. Journal of Water Process Engineering, 38, 101575. https://doi.org/10.1016/j.jwpe.2020.101575

Bian, S., Wang, Y., Xiao, F., Tong, Y., Gao, C., & Zhu, G. (2022). Fabrication of polyamide thin-film nanocomposite reverse osmosis membrane with improved permeability and antibacterial performances using silver immobilized hollow polymer nanospheres. Desalination, 539, 115953. https://doi.org/10.1016/j.desal.2022.115953

Fahrina, A., Arahman, N., Aprilia, S., Bilad, M. R., Silmina, S., Sari, W. P., Sari, I. M., Gunawan, P., Pasaoglu, M. E., Vatanpour, V., Koyuncu, I., & Rajabzadeh, S. (2022). Functionalization of PEG-AgNPs hybrid material to alleviate biofouling tendency of polyethersulfone membrane. Polymers, 14(9), 1–17. https://doi.org/10.3390/polym14091908

Gan, J. Y., Chong, W. C., Sim, L. C., Koo, C. H., Pang, Y. L., Mahmoudi, E., & Mohammad, A. W. (2020). Novel carbon quantum dots/silver blended polysulfone membrane with improved properties and enhanced performance in tartrazine dye removal. Membranes, 10(8), 1–18. https://doi.org/10.3390/membranes10080175

He, M., Li, W.-D., Chen, J.-C., Zhang, Z.-G., Wang, X.-F., & Yang, G.-H. (2022). Immobilization of silver nanoparticles on cellulose nanofibrils incorporated into nanofiltration membrane for enhanced desalination performance. NPJ Clean Water, 5(1), 64. https://doi.org/10.1038/s41545-022-00217-7

Huq, M. A., Ashrafudoulla, M., Rahman, M. M., Balusamy, S. R., & Akter, S. (2022). Green synthesis and potential antibacterial applications of bioactive silver nanoparticles: A review. Polymers, 14(4), 1–28. https://doi.org/10.3390/polym14040742

Jyoti, K., Baunthiyal, M., & Singh, A. (2016). Characterization of silver nanoparticles synthesized using Urtica dioica Linn. leaves and their synergistic effects with antibiotics. Journal of Radiation Research and Applied Sciences, 9(3), 217–227. https://doi.org/10.1016/j.jrras.2015.10.002

Li, Q., Mahendra, S., Lyon, D. Y., Brunet, L., Liga, M. V., Li, D., & Alvarez, P. J. J. (2008). Antimicrobial nanomaterials for water disinfection and microbial control: Potential applications and implications. Water Research, 42(18), 4591–4602. https://doi.org/10.1016/j.watres.2008.08.015

Little Flower, N. A., Rahulan, K. M., Sujatha, R. A., Sharath, R. A., Darson, J., & Gopalakrishnan, C. (2019). Fabrication of silver nanoparticles decorated polysulfone composite membranes for sulfate rejection. Applied Surface Science, 493, 645–656. https://doi.org/10.1016/j.apsusc.2019.06.281

Mino, Y., Fukukawa, N., & Matsuyama, H. (2021). Simulation on pore formation from polymer solution at surface in contact with solid substrate via thermally induced phase separation. Membranes, 11(7), 1–15. https://doi.org/10.3390/membranes11070527

Mohamad Said, K. A., Ismail, A. F., Zulhairun, A. K., Abdullah, M. S., Azali, M. A., & Zainal Abidin, M. N. (2022). Magnetic induced asymmetric membrane: Effect of magnetic pattern to phenol removal by adsorption. Materials Chemistry and Physics, 278, 125692. https://doi.org/10.1016/j.matchemphys.2021.125692

Mollahosseini, A., Rahimpour, A., Jahamshahi, M., Peyravi, M., & Khavarpour, M. (2012). The effect of silver nanoparticle size on performance and antibacteriality of polysulfone ultrafiltration membrane. Desalination, 306, 41–50. https://doi.org/10.1016/j.desal.2012.08.035

Parsamehr, P. S., Zahed, M., Tofighy, M. A., Mohammadi, T., & Rezakazemi, M. (2019). Preparation of novel cross-linked graphene oxide membrane for desalination applications using (EDC and NHS)-activated graphene oxide and PEI. Desalination, 468, 114079. https://doi.org/10.1016/j.desal.2019.114079

Pereira, L., Mondal, P. K., & Alves, M. (2015). Aromatic amines: Sources, environmental impact and remediation. In E. Lichtfouse, J. Schwarzbauer, & D. Robert (Eds.), Pollutants in Buildings, Water and Living Organisms (pp. 297–346). Springer. https://doi.org/10.1007/978-3-319-19276-5_7

Prihandana, G. S., Sriani, T., Muthi'ah, A. D., Musa, S. N., Jamaludin, M. F., & Mahardika, M. (2022). Antibacterial activity of silver nanoflake (SNF)-blended polysulfone ultrafiltration membrane. Polymers, 14(17), 1–14. https://doi.org/10.3390/polym14173600

Rai, M., Ingle, A. P., Trzcińska-Wencel, J., Wypij, M., Bonde, S., Yadav, A., Kratošová, G., & Golińska, P. (2021). Biogenic silver nanoparticles: What we know and what do we need to know? Nanomaterials, 11(11), 1–29. https://doi.org/10.3390/nano11112901

Theivasanthi, T., & Alagar, M. (2011). Electrolytic synthesis and characterizations of silver nanopowder. arXiv, 1–10. https://doi.org/10.48550/arXiv.1111.0260

Vatanpour, V., Keskin, B., Naziri Mehrabani, S. A., Karimi, H., Arabi, N., Behroozi, A. H., Shokrollahi-Far, A., Yavuzturk Gul, B., & Koyuncu, I. (2022). Investigation of boron nitride/silver/graphene oxide nanocomposite on separation and antibacterial improvement of polyethersulfone membranes in wastewater treatment. Journal of Environmental Chemical Engineering, 10(1), 107035. https://doi.org/10.1016/j.jece.2021.107035

Wu, X., Fang, F., Zhang, B., Wu, J. J., & Zhang, K. (2022). Biogenic silver nanoparticles-modified forward osmosis membranes with mitigated internal concentration polarization and enhanced antibacterial properties. NPJ Clean Water, 5(1), 41. https://doi.org/10.1038/s41545-022-00190-1

Zambare, R. S., Dhopte, K. B., Patwardhan, A. V., & Nemade, P. R. (2017). Polyamine functionalized graphene oxide polysulfone mixed matrix membranes with improved hydrophilicity and anti-fouling properties. Desalination, 403, 24–35. https://doi.org/10.1016/j.desal.2016.02.003

Zeng, Q., Wan, Z., Jiang, Y., & Fortner, J. (2022). Enhanced polysulfone ultrafiltration membrane performance through fullerol addition: A study towards optimization. Chemical Engineering Journal, 431, 134071. https://doi.org/10.1016/j.cej.2021.134071

Zhao, Z., Li, P., Xie, R., Cao, X., Su, D., & Shan, Y. (2022). Biosynthesis of silver nanoparticle composites based on hesperidin and pectin and their synergistic antibacterial mechanism. International Journal of Biological Macromolecules, 214, 220–229. https://doi.org/10.1016/j.ijbiomac.2022.06.048

